JOURNAL OF Materials CHEMISTRY

In situ investigation of the thermal decomposition of Co–Al hydrotalcite in different atmospheres

Javier Pérez-Ramírez,* Guido Mul, Freek Kapteijn and Jacob A. Moulijn

Industrial Catalysis, DelftChemTech, University of Technology, Julianalaan 136, 2628 BL Delft, The Netherlands. E-mail: j.perezramirez@tnw.tudelft.nl; Fax: +31 (0)15 278 4452; Tel: +31 (0)15 278 4356

Received 20th November 2000, Accepted 20th December 2000
First published as an Advance Article on the web 7th February 2001

High temperature X-ray diffraction (HT-XRD), thermal analysis (TGA-DTA), mass spectrometry (MS), *in situ* Fourier transform infrared (FT-IR) spectroscopy, and *in situ* Raman spectroscopy have been used to characterize the thermal decomposition of Co–Al hydrotalcite, $[Co_6Al_2(OH)_{16}](CO_3)\cdot 4H_2O$, in air and inert atmospheres. In the first decomposition step, water is removed from the structure, a process which is complete at 150–200 °C. This transition is followed by dehydroxylation and decarbonation, as well as carbonate reorganization in the interlayer space. These processes require higher temperatures under inert atmospheres than in air. The transition temperatures also depend on the nature of the technique applied (static *vs.* dynamic operation). An intermediate metastable mixture of phases is identified, which contains the dehydrated layered structure and an emerging spinel-like mixed oxide phase. This phase is formed in the region of 150–175 °C in air and was not observed under inert atmospheres. Dehydroxylation leads to the collapse of the hydrotalcite phase and is complete at 250–300 (air) and 350–400 °C (inert gas). Carbonate removal is coupled with the dehydroxylation process, although removal of carbonate groups is only complete at 450 (air) and 600 °C (inert gas). Thermal treatment in air finally leads to a solid solution of cobalt spinels $[Co(Co,Al)_2O_4]$. Mixtures of CoO and $CoAl_2O_4$ are formed upon treatment under inert atmospheres. Based on the analytical results, a simplified structural model for the decomposition process is presented. The presence of oxidizable Co^{2+} cations in the octahedral sheets and the diffusion of Co^{3+} to the interlayer space in the dehydrated layered structure, and the stability of the solid solution of Co-spinels formed are identified as key factors in the low thermal stability of the hydrotalcite precursor in air.

Introduction

Hydrotalcite-like compounds (HTlcs) have attracted much attention in recent years as catalyst precursors and catalyst supports.[1–12] This is due to (i) their ability to accommodate a large variety of bivalent and trivalent cations, (ii) the homogeneous mixture of the cations on an atomic scale, and (iii) the formation of thermostable mixed oxides with a high surface area, often denoted as ex-HTlcs, upon decomposition. The first two properties are a result of the precursor, while the last property appears to be related to the decomposition mechanism.[13,14]

Synthetic HTlcs, with the general formula $[M^{2+}_{1-x}M^{3+}_{x}(OH)_2][A^{m-}]_{x/m}\cdot nH_2O$, are hydrated hydroxycarbonates of random lamellar structure. These materials can be visualized as brucite-type octahedral layers, in which M^{3+} cations partially substitute for M^{2+} cations ($x = M^{3+}/M^{2+}+M^{3+}$). The cations are located in the center of the octahedron formed by six hydroxyl groups. The metal octahedra share edges to form two-dimensional infinite sheets, similar to brucite $[Mg(OH)_2]$. The brucite-like layers can stack to build a tridimensional network and are linked by various chemical interactions (mainly hydrogen bonding) between the sheets. The positive charge resulting from this substitution is balanced by anions (often carbonate), together with water molecules arranged in interlayers alternating with the octahedral sheets. The structure as outlined above was first described by Allman[15] and Taylor.[16]

Monitoring structural changes during thermal decomposition of HTlcs has been the aim of numerous studies. The interpretation of the decomposition process is often based merely on the information obtained from *ex situ* X-ray diffraction, thermal analysis (TGA combined with DTA or DSC), and gas physisorption experiments.[17–19] An integration of suitable techniques and experimental procedures is usually not applied. Furthermore, most of the studies published on calcined hydrotalcites are carried out at room temperature, where the state of the sample may have changed during cooling, exposure to the atmosphere and handling. ^{27}Al MAS-NMR has been used to study the cation coordination upon heating,[14,17,20–22] however, due to the *ex situ* nature of this technique, certain rehydration of the partially decomposed materials cannot be excluded. Spectroscopic techniques have rarely been used to investigate the decomposition, and experiments were usually performed in vacuum or *ex situ*.[20,23,24] Kloprogge and Frost[25] have applied *in situ* IES (infrared emission spectroscopy) to assess the spinel formation upon decomposition of Mg, Co and Ni-HTlcs, but the low temperature range (<200 °C) could not be investigated due to the nature of the IES technique. The limitations of this technique have been discussed recently.[26] HT-XRD has been used as one of the few *in situ* techniques to investigate the decomposition and reconstruction mechanism over Mg–Al-HTlc.[14,21,22] Belloto *et al.*[14] also used *in situ* anomalous diffraction and EXAFS to study the decomposition process of Mg-based HTlcs in order to explain the remarkable thermal stability of the decomposed materials.

Recently, we investigated the high resistance of Co–Al-HTlc towards reconstruction after calcination at 200 °C.[27] This extraordinary property has been related to the

decomposition mechanism of the material, which differs greatly from that of other layered double materials, like Mg–Al or Ni–Al-HTlcs. In this paper, we describe a model for the thermal decomposition mechanism of Co–Al-HTlc in air and inert atmospheres, which is based on the results of a combination of *in situ* techniques (HT-XRD, TGA-DTA, MS, FT-IR spectroscopy, and Raman spectroscopy). To the best of our knowledge, besides the contributions of Kloprogge and Frost,[25] application of *in situ* vibrational spectroscopies to investigate the decomposition of hydrotalcites has not been reported elsewhere.

Experimental

Material preparation

Co–Al hydrotalcite was prepared by co-precipitation at static pH and temperature at low supersaturation conditions, as previously described.[2] A flow ($2\,l\,h^{-1}$) of an aqueous solution of the metal nitrates [$Co(NO_3)_2{\cdot}6H_2O$, >99.0%, Merck and $Al(NO_3)_3{\cdot}9H_2O$, >99.0%, Fluka] in the desired molar ratio [$x = Al^{3+}/(Co^{2+} + Al^{3+}) = 0.25$] with a total cation concentration of 1.5 M was mixed slowly at 22 °C under vigorous agitation with an alkaline solution of Na_2CO_3/NaOH, with a carbonate concentration in the molar CO_3^{2-}/Al^{3+} ratio of 2. The pH of the mixtures was kept at 9.5 by adjusting the flow rate of the alkaline solution. Following this addition, the slurry was aged at 65 °C for 18 h under mild stirring. A reflux unit was mounted on top of the vessel to prevent water evaporation. Finally, the material was cooled to room temperature, filtered, washed with a large volume of warm (30 °C) deionized water until the Na^+ had been completely removed (<0.01 vol%) and dried at 90 °C for 12 h.

Material characterization

The chemical composition of the as-synthesized material was determined by inductively coupled plasma optical emission spectroscopy (ICP-OES) [Perkin-Elmer Plasma 40 (Si) and Optima 3000DV (axial)].

High temperature X-ray diffraction (HT-XRD) analysis was carried out with a STOE diffractometer in Bragg–Brentano geometry, using Cu-Kα radiation ($\lambda = 0.154$ nm) and a diffracted beam graphite monochromator. A high temperature cell was installed, enabling *in situ* experiments under a controlled atmosphere to be performed. Samples were mounted on a stainless steel plate by placing a few droplets of a suspension of ground and sieved sample (75–100 μm) in ethanol on the plate, followed by drying at ambient conditions. The measurements were performed under flowing air or N_2 (50 ml min^{-1}), and with samples of around 10 mg. The gas flow was positioned across the sample, thus ensuring good solid–gas contact. The patterns were measured after 1 h equilibration at each temperature, in the range 30–500 °C. The heating rate used was 10 °C min^{-1}. Measurement conditions were: 2θ range 5–70°, step size 0.034° 2θ and step counting time 2 s. The observed interplanar d spacing was corrected using elemental Si as an internal standard [$d(111) = 0.313$ nm; JCPDS no. 27-1402].

The parameter a of the layered structure corresponds to the average cation–cation distance within the layers and can be calculated as $a = 2 \times d(110)$.[1] The c parameter, which is related to the thickness of the brucite-like layer and the interlayer distance, is commonly calculated as $c = 3 \times d(003)$, assuming a 3R polytypism for the hydrotalcite.[28] This computation is applicable if the $d(00l)$ reflections are sharp. However, if the peaks are somewhat broad, it has been proposed that c can be better determined by averaging the position of the diffraction peaks corresponding to the (003), (006) and (009) planes,[29] according to eqn. 1 and 2.

$$c/3 = 1/2 \times (d(003) + (2 \times d(006))) \quad (1)$$

$$c/3 = 1/2 \times (d(003) + (2 \times d(006)) + (3 \times d(009))) \quad (2)$$

The Scherrer equation, $\bar{L} = 0.9\lambda/\beta\cos\theta$, was used to estimate the crystallite size of the decomposed materials, where $\bar{L}$ is the volume-averaged thickness of the crystallites, measured in a direction normal to the reflection planes, λ is the wavelength of the radiation used, β is the full width at half-maximum (fwhm) in radians, and θ is the Bragg diffraction angle (experimental). The (440) and (220) reflection planes in the pattern of the oxide, were used to determine the β value during decomposition in air and under inert atmospheres, respectively.

Thermal analysis (TGA-DTA) was carried out using a Mettler-Toledo TGA/SDTA 851 apparatus equipped with a sample robot and a gas controller for air or inert gas (He). The solid (*ca.* 25 mg sample, no dilution, particle size 75–100 μm) was placed in an alumina crucible (70 μl) using α-Al_2O_3 as reference. Tests were performed in dry air and helium flow of 100 cm^3 min^{-1} STP at atmospheric pressure. The temperature was increased from 25 to 1000 °C with a heating rate of 10 °C min^{-1}. For the experiment in inert gas, a pre-purge step in He (100 cm^3 min^{-1}) at room temperature was applied for 1 h in order to remove the remaining air in the reaction chamber.

The evolution of the gases during the decomposition of Co–Al-HTlc (in air or nitrogen) were analyzed on-line by a computer-controlled quadrupole mass spectrometer (MS) (Balzers Quadstar 421). 50 mg of the as-synthesized material (particle size 75–100 μm) was decomposed in air or N_2 flow (100 cm^3 min^{-1} STP) in a quartz tube fixed-bed reactor of 5 mm inner diameter. The temperature was raised from room temperature to 700 °C at 10 °C min^{-1}. The reactor and the spectrometer were coupled through a heated capillary sampling tube (length = 80 cm, inner diameter = 0.15 mm, $T = 385$ K). Masses analyzed were m/z 18 (H_2O), 28 (CO), and 44 (CO_2).

The *in situ* Fourier transform infrared (FT-IR) spectra were recorded using a Spectratech diffuse reflectance (DRIFT) accessory and a Nicolet Magna 550 Fourier transform spectrometer. The transitions during thermal activation were studied *in situ* by placing the sample on a holder (*ca.* 20 mg of hydrotalcite) in a reaction chamber under air or nitrogen flow (25 cm^3 min^{-1} STP). The spectra were collected in the range 25–550 °C at random intervals of 25 or 50 °C, using a heating rate of 10 °C min^{-1}. The spectra were recorded after reaching every set-point, by co-addition of 256 scans (approximate scanning time 300 s), with a nominal resolution of 4 cm^{-1}.

The *in situ* visible Raman spectra were obtained using a Renishaw Raman Imaging Microscope, system 2000, using a 20 mW Ar^+ laser ($\lambda = 514$ nm). The Ramascope was calibrated using a silicon wafer. The focus (maximum opening at 100%) and the power (10%) were carefully optimized beforehand in order not to alter the sample by exposure to the laser. The transitions during thermal activation were studied *in situ* by placing the sample (*ca.* 20 mg of hydrotalcite) in a high temperature cell (Linkam TS1500) in flowing air or nitrogen (25 cm^3 min^{-1} STP). The spectra were collected in the range 25–550 °C at random intervals at a heating rate of 10 °C min^{-1}. To improve the signal-to-noise ratio, a recording time of 120 s and 2 accumulations were applied.

Results and discussion

Chemical composition

The analysis of the hydrotalcite-like compound by ICP-OES revealed that the ratio between cations in the sample (Co : Al = 2.9 : 1) was close to that in the starting solution (Co : Al = 3 : 1), hence the co-precipitation step was carried out effectively.

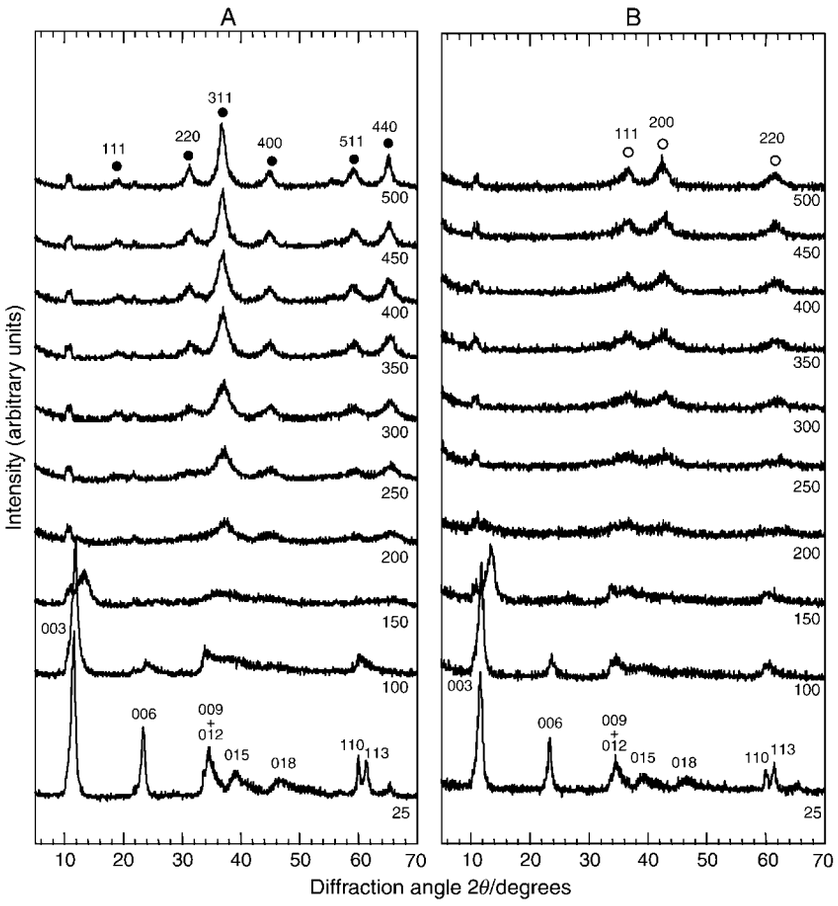

Fig. 1 HT-XRD patterns for the thermal decomposition of Co–Al-HTlc (Co : Al = 3 : 1) in (A) air and (B) inert gas (N_2) at different temperatures (in °C), as indicated in the figure. Crystalline phases in the decomposed products: (●) cobalt spinel; (○) CoO.

High-temperature X-ray diffraction

The HT-XRD patterns (Fig. 1) at room temperature (both in air and under nitrogen flow) show the hydrotalcite structure as the only crystalline component (JCPDS file no. 22-700), exhibiting sharp and symmetric reflections of the basal (003), (006), and (009) planes, and broad and asymmetric reflections for the non-basal (012), (015), and (018) planes. The (009) and (012) reflections overlap result in the broad signal between 32 and 38° 2θ. Furthermore, the two reflections of (110) and (113) can be clearly distinguished around 60° 2θ. The cell parameters a and c of the layered structure are 0.308 and 2.286 nm, respectively. The positions of the first two sharp peaks were used for the calculation of c (see experimental section, eqn. 1).

Upon heating of the layered double material from 25 to 100 °C in air (Fig. 1A), the reflection of the basal spacing d(003) shifts slightly to lower d values, from 0.762 to 0.749 nm. This is a result of the removal of physically adsorbed water and the partial release of interlayer water from the hydrotalcite, causing a slight decrease in the interlayer spacing. It should be noted that in the patterns at 100 °C, the intensity of the second harmonic reflections, planes (006) and (009), decreases much more than the intensity of planes (003). The resolution of the doublet close to 60° 2θ is also worse, and the (113) reflection vanishes, while the intensity of the (110) reflection diminishes significantly, becoming broader. In the pattern at 150 °C, only the (003) reflection of the hydrotalcite phase is visible. At this temperature, removal of interlayer water is complete. This reflection appears at d(003) = 0.658 nm in air, indicating a change in the cell parameter c from 2.286 nm at room temperature to 1.974 nm at 150 °C in the dehydrated structure. Overall, it can be concluded that the sample partially retains a layered structure in both air and inert atmospheres at this temperature, with similar metal–metal distances in the layer as in the parent sample.[29] However, the disappearance of the (006) and (009) planes indicates disorder in the stacking of the layers, as previously stated by other authors.[22,30] The distortion of the (00l) reflections upon heating of the sample from room temperature to 100 °C, and further to 150 °C, indicates the removal of interlayer water in the c direction, deteriorating the basal reflections. The reflection at around 11° 2θ in both HT-XRD patterns for the materials heated in air and N_2 above 150 °C is an artefact caused by the sample holder, as was concluded after recording the diffraction pattern in the absence of a sample at different temperatures.

At 150 °C, new broad reflections at 2θ values around 36 and 65° 2θ can be identified in the pattern measured in air. The same pattern was obtained after an additional 2 h at this temperature. The formation of an intermediate metastable phase, a mixture of the emerging mixed oxide phase and the dehydrated HTlc, suggests that dehydroxylation of the layers has occurred to a certain extent at this temperature. At 200 °C, the hydrotalcite structure collapses completely. All the new reflections in the pattern indicate the presence of poorly crystallized spinel-like mixed oxide. As the heating temperature is increased, the crystallinity of the oxide phase formed is enhanced, as indicated by sharpening of the XRD lines.

The HT-XRD patterns in inert gas (N_2) (Fig. 1B) show a similar trend as in air. In both cases, the dehydrated layered structure appears at 150 °C and collapses at 200 °C. However, significant differences compared to decomposition in air can be identified. In an inert atmosphere, characteristic basal reflections of the layered phase can still be observed at 150 °C, *i.e.* planes (012) and (110), which were not identified in the presence of air at that temperature. In addition, the intensity of the basal (003) reflection is stronger in inert gas at 150 °C. In the sample decomposed in N_2, the intermediate metastable mixture of

phases could not be identified in the HT-XRD patterns at 150 °C or higher, going from the dehydrated layered structure to the oxide phase. These features indicate a higher thermal stability of the layered structure upon heating in inert gas and should certainly be related to differences in the decomposition mechanism under both types of atmosphere.

Another difference related to the decomposition process in air and inert gas is the formation of the single oxide CoO in N_2, appearing as the only crystalline phase. According to the literature, CoO is not a stable phase in the presence of oxygen at temperatures between 325 and 725 °C.[31] In our case, we could not identify CoO in the structure at any temperature during decomposition in air. Apart from the CoO phase, the remaining part of the cation in excess (Co^{2+}) and Al^{3+} should lead to the formation of $CoAl_2O_4$. Since the diffraction pattern of the oxide phase after decomposition in N_2 only shows CoO as the crystalline phase, an amorphous $CoAl_2O_4$ phase is apparently present.

The diffraction patterns during decomposition in air suggest the presence of a cobalt spinel phase. From the XRD analysis it is impossible to distinguish between Co_3O_4, $CoAl_2O_4$, and Co_2AlO_4 due to the almost identical positions of the various reflections. Co and Al mixed oxides usually lead to normal spinels, $CoAl_2O_4$-type, where Co^{2+} occupies tetrahedral positions and Al^{3+} fills the octahedral positions. It is thus unlikely that the inverse spinel is formed, although this cannot be completely excluded. A TEM micrograph of the sample calcined at 200 °C (not shown here) revealed the presence of a crystalline oxide phase. Amorphous regions could not be identified. This may indicate an intimate dissolution of Al^{3+} in the main Co_3O_4 phase (due to the molar Co/Al ratio in the as-synthesized material), as was previously suggested by Kannan and Swamy.[32] In this case, Al^{3+} isomorphically substitutes Co^{3+} in the Co_3O_4 phase, leading to a very homogeneous and stable spinel-like mixed oxide. This solid solution phase is denoted $Co(Co,Al)_2O_4$ herein.

The cell parameter of the oxide phase was calculated from the (440) plane of the experimental patterns at different temperatures after cooling to room temperature and measuring to avoid thermal expansion effects in the cell at high temperature and to improve the quality of the XRD patterns recorded. The result, displayed in Fig. 2, shows the continuous increase of the *a* value with increasing temperature. In the same figure, the cell parameters reported for the pure spinels are also indicated. The progressive increase of the lattice parameter is in agreement with the formation of a solid solution of cobalt spinels. The *a* value is below those reported for pure spinels in the range of temperatures investigated, which also indicates the formation of non-stoichiometry, in the form of anion vacancies and/or dissolution of Al^{3+} ions in the spinel phase.[32]

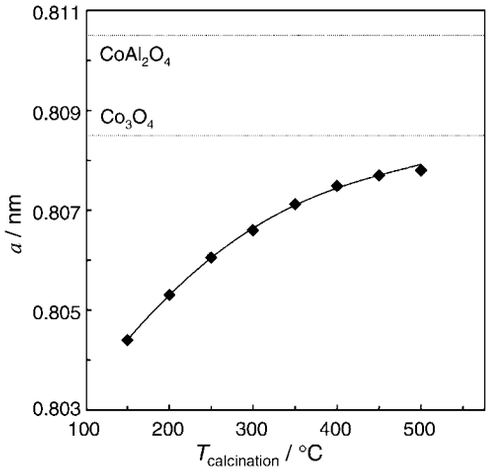

Fig. 2 Evolution of lattice parameter *a* with temperature for the spinel-like phase obtained during decomposition of Co–Al-HTlc (Co : Al = 3 : 1) in air from *ex situ* measurements. Dashed lines represent the cell parameters for Co_3O_4 ($a = 0.808$ nm, JCPDS 43-1003) and $CoAl_2O_4$ ($a = 0.810$ nm, JCPDS 44-160).

HT-XRD also provides semi-quantitative information about the morphology of the crystalline phases formed after decomposition. In this sense, the average crystal size of the oxide phases formed is larger in air than in an inert atmosphere, 5.4 *vs.* 3.7 nm, respectively, as calculated from the Scherrer formula (see experimental section). This suggests the tendency of $Co(CoAl)_2O_4$ to sinter, while in the XRD pattern at 450 °C in an inert atmosphere, the CoO phase may remain dispersed on an amorphous $CoAl_2O_4$ phase, which acts as a support. This result is in agreement with previous studies on Co–Al mixed oxides,[33] although it should be confirmed by a detailed electron microscopic analysis.

Thermal analysis and mass spectrometry

The decomposition profiles as determined by TGA-DTG-DTA in air and inert gas, as well as the analysis of the evolved decomposition products by MS are presented in Fig. 3 and 4, respectively. The thermogravimetric profiles show the occurrence of the decomposition in two main steps in both air and inert gas (I and II in Fig. 3), as typically observed for layered double materials.[19,34–36] The maximum peaks of the DTA profile and of the derivative of the weight loss (DTG) profile are in excellent agreement, as is shown in Table 1. Interpretation of the TGA-DTA data is based on the MS analysis of the evolved gases (Fig. 4). Two overlapping *m*/*z* 18 signals can be observed in both air and inert gas, which is assigned to the removal of interlayer water (transition I in the DTA profile) and dehydroxylation of the brucite-like sheets (transition II), respectively. CO_2 evolution also occurs in various temperature stages. The first evolution is related to physically adsorbed CO_2. A strong *m*/*z* 44 signal is observed around 265 °C (transition II), suggesting decarbonation, which is coupled to the dehydroxylation stage. In inert gas, the maximum signal *m*/*z* 44 at 260 °C, due to decarbonation, is located at slightly lower temperatures than the *m*/*z* 18 signal at 272 °C, indicating dehydroxylation. At higher temperatures, an additional weak and broad *m*/*z* 44 signal appears (around 375 °C). This is probably related to the residual weight loss observed at $T > 350$ °C in the TGA-DTA profiles (Fig. 3). A peak at *m*/*z* 28, corresponding to CO, was not observed along the whole temperature range for the two atmospheres employed.

In the sample decomposed in air, the simultaneous occurrence of the different processes appears as a single-step weight loss in the TGA profile. In inert gas the main transitions appear to be more separated, and a two-step weight loss occurs. The maxima in the DTG and DTA profiles of transitions I and II in air are separated by 40 °C, while in the case of the sample in nitrogen the difference is 85 °C. This is confirmed by the MS analysis. Apparently, the weight loss for transition I is higher for the sample in air than in nitrogen and that for transition II is lower (see Table 1). The total weight loss of the as-synthesized material was similar in both atmospheres (*ca.* 32 wt.%).

In situ FT-IR spectroscopy

Infrared spectra were recorded both during the decomposition of Co–Al-HTlc in air and inert gas (Fig. 5). Spectral assignments will be extensively discussed elsewhere.[37] In the spectrum at room temperature in air, the absorption band at 3545 cm^{-1} is attributed to the H-bonding stretching vibrations of the hydroxyl group and the stretching vibration of water molecules.[1] The shoulder present at 3050 cm^{-1} has been attributed to hydrogen bonding between H_2O and the anion in the interlayer space ($HOH\cdots CO_3^{2-}$).[38–40] The H_2O bending

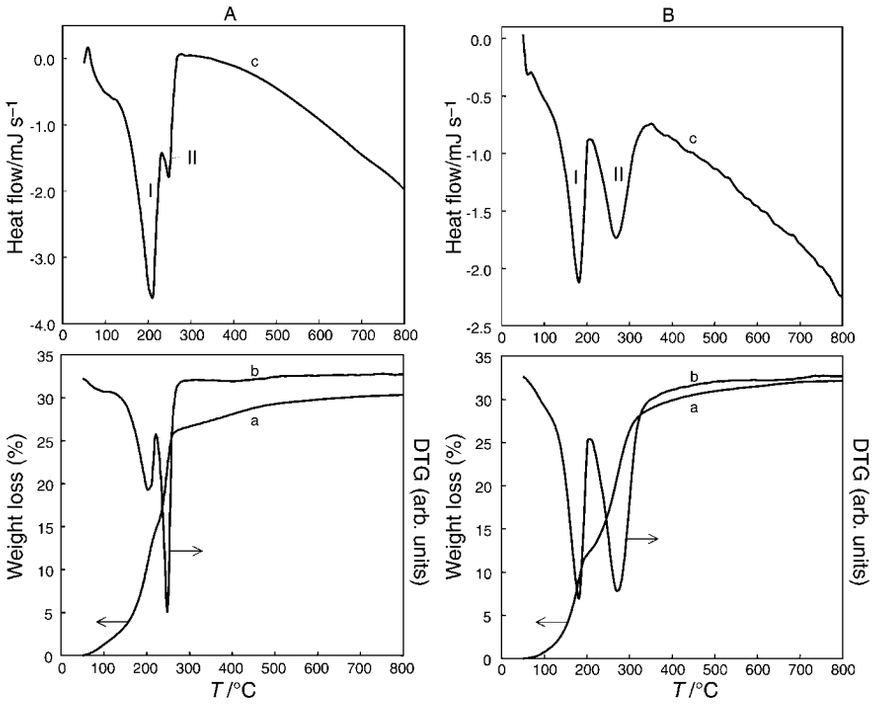

Fig. 3 (a) Thermal gravimetric analysis (TGA), (b) differential gravimetric analysis (DTG), and (c) differential thermal analysis (DTA) profiles for the decomposition of Co–Al-HTlc (Co : Al = 3 : 1) in (A) air and (B) inert gas (He).

vibration is located at 1650 cm^{-1}. We assign the shoulder observed at 1750 cm^{-1} in the spectra at room temperature (both in air and inert gas) to a restricted bending mode of water in the interlayer space.[37] This band should indeed be related to interlayer water, since it disappears at 200 °C, *i.e.* when the double layered structure is dehydrated.

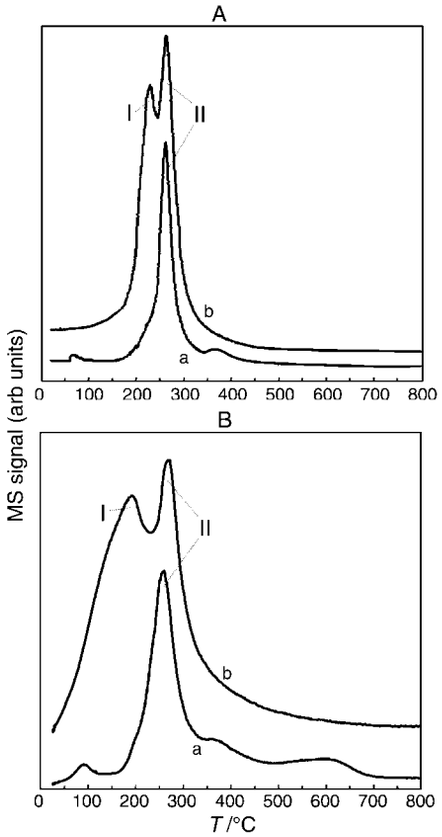

Fig. 4 MS profiles of the evolved gases (a) *m*/*z* 44 and (b) *m*/*z* 18, during the decomposition of Co–Al-HTlc (Co : Al = 3 : 1) in (A) air and (B) inert gas (N_2).

The main absorption bands in the carbonate region are located between 1200 and 1700 cm^{-1}. The carbonate anion in a symmetric environment is characterized by a D_{3h} (planar) symmetry and has three infrared absorption bands at frequencies close to those of the "free ion": 1415 (ν_3, asymmetric stretching), 880 (ν_2, out-of-plane deformation), and 680 cm^{-1} (ν_4, in-plane bending).[41] In the infrared spectrum of the as-synthesized material, the vibrational modes ν_3 at 1414 cm^{-1} and ν_2 at 835 cm^{-1} were identified. The ν_4 carbonate vibration is not clearly observed in our spectra. The presence of a shoulder at 1380 cm^{-1} is a result of the splitting of the ν_3 mode, indicating a lowering in the symmetry of the carbonate, as well as the disordered nature of the interlayer space.[40]

In the low wavenumber region (< 1000 cm^{-1}) information about the octahedral layers of the HT structure can be obtained. The band centered at 625 cm^{-1} is assigned to Co–O stretching in the brucite-like sheet, while the band at 471 cm^{-1} is due to Al–O stretching.[25,39] The band at 955 cm^{-1} is assigned to an Al–OH deformation.[23]

The first changes upon heating in the spectra presented in Fig. 5A occur from 25 to 100 °C. A decrease in intensity of the band centered at 1650 cm^{-1} is observed, which is related to the loss of physically adsorbed water. In this temperature range, there is also a slight decrease in intensity of the shoulders at 1750 and 3050 cm^{-1} indicating partial removal of interlayer water. The shoulders at 1650, 1750, and 3050 cm^{-1} disappear completely at 200 °C. Furthermore, the carbonate band at 1415 cm^{-1} in the original hydrotalcite splits into two new bands at 1350 and 1570 cm^{-1} (splitting of the ν_3 mode) at 200 °C, indicating a rearrangement of carbonate in the interlamellar space. This reorganization of the carbonate anion leads to a further lowering of the symmetry, inducing absorption at the position of the ν_1 mode (symmetrical stretching) at 1030 cm^{-1}. This vibrational mode is inactive when the carbonate ion retains its full symmetry.[42]

In the temperature range 200–250 °C, tremendous dehydroxylation occurs, most likely by condensation between layers. Significant decarbonation also occurs, indicating a coupling and simultaneous occurrence of both processes. This result suggests a crucial role of the intermediate dehydrated

Table 1 Transition temperatures and weight losses during decomposition of Co–Al-HTlc in air and inert gas, as determined by TGA-DTG-DTA and MS analyses

	Air		Inert gas (He)	
Technique	I[a]	II[b]	I[a]	II[b]
TGA (wt.%)	14.5	15.7	12.7	19.4
DTG/°C	208	249	182	268
DTA/°C	210	249	183	270
MS/°C	230	264	190	260–272

[a]Transition I: removal of interlayer water. [b]Transition II: dehydroxylation and decarbonation.

structure in the carbonate symmetry and intralayer bonding in approaching the final decomposed material, as anticipated by Belloto *et al.*[14] The doublet carbonate band decreases in intensity and shifts to lower frequencies (to 1533 and 1304 cm^{-1}, respectively).

The spectrum at 200 °C shows a shoulder at around 700 cm^{-1}, and the band at 955 cm^{-1} shifts to lower frequencies (*ca.* 900 cm^{-1}). This indicates the start of the collapse of the double-layered structure and the formation of the spinel-like structure. The original band at 625 cm^{-1} is overlapped by the 700 cm^{-1} band due to the emerging phase, while the band at 471 cm^{-1} is hardly visible. The simultaneous presence of absorption bands typical of hydrotalcite and mixed oxide suggests the presence of the intermediate metastable mixture of phases, which was also observed in the HT-XRD pattern of the sample decomposed in air at 150 °C. The transition of the layered structure to the mixed oxide involves shifting of the bands at 955 and 621 cm^{-1} to lower wavenumbers. At 250 °C, a doublet centered at 725 and 609 cm^{-1} appears, typical of a normal II–III spinel compound, indicating loss of lamellar arrangement and the collapse of the layered structure. The spinel formation takes place while some carbonate is still present, indicating the collapse of the layered structure occurs before complete decarbonation. At 300 °C, the doublet due to the spinel-like mixed oxide is better defined. The bands observed are shifted with respect to the data reported for pure spinel compounds.[43] This is in agreement with the presence of a solid solution of cobalt spinels. The investigations of solid solutions, even simple types of binary compounds with cubic symmetry, have led to complex interpretations of the vibrational behaviour, by modification, shifting, or splitting of band positions.[43]

The processes in air and inert gas show important differences, although the positions of the different absorption bands are similar in both cases (compare Fig. 5A and B). In air, increasing the temperature from 200 to 250 °C induces extensive dehydroxylation and decarbonation. However, dehydroxylation only occurs between 300–350 °C in inert gas, and carbonates are still present in the material even above 550 °C. These differences are in agreement with the overlap of transitions I and II in air and the separation of these transitions observed in inert gas, as previously shown in the TGA-DTA and MS analysis (Fig. 3 and 4). In the low wavenumber region, the collapse of the layered structure and the formation of the oxide phase is observed in air at 250–300 °C, while 350 °C is needed when an inert gas atmosphere is employed.

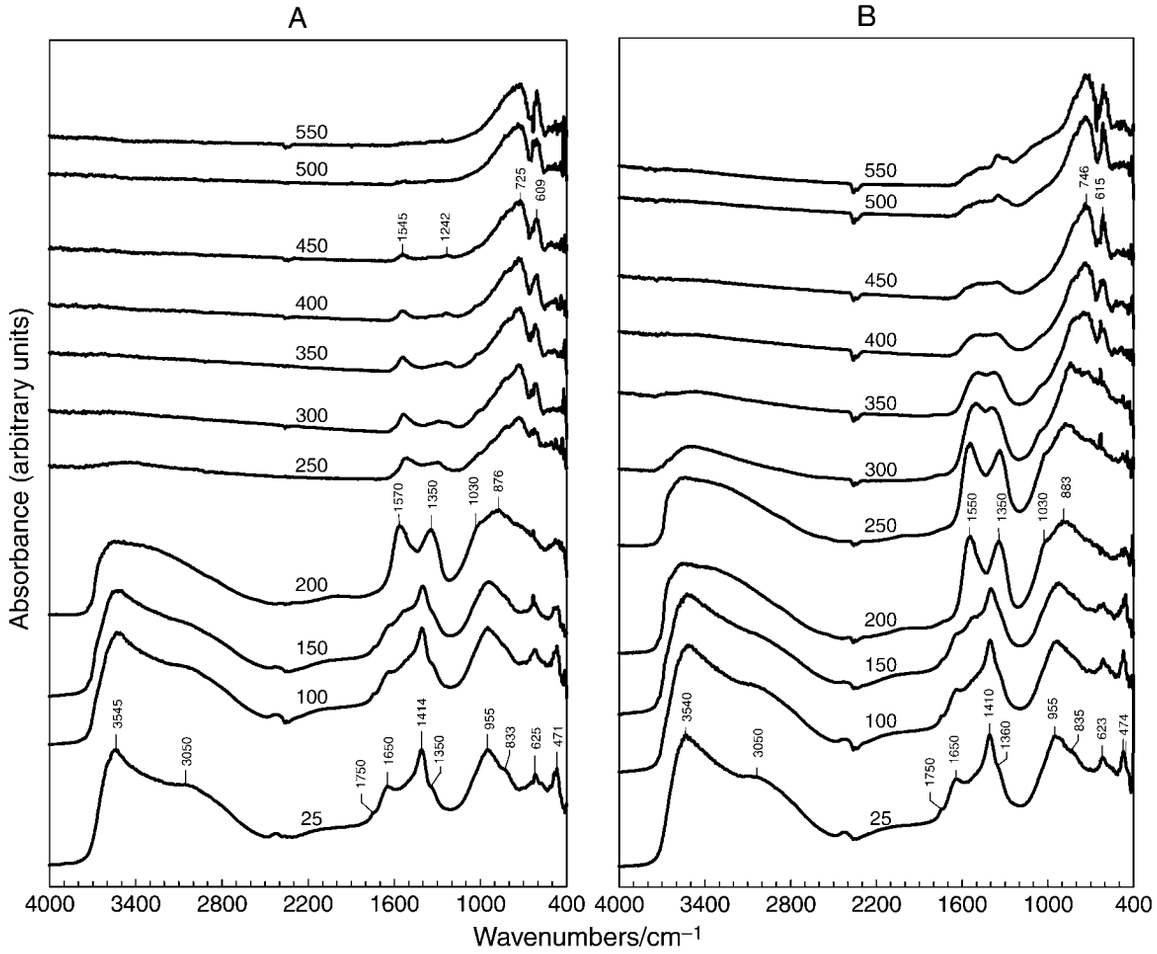

Fig. 5 *In situ* FT-IR spectra for the thermal decomposition of Co–Al-HTlc (Co : Al = 3 : 1) in (A) air and (B) inert gas (N_2) at different temperatures (in °C), as indicated in the figure.

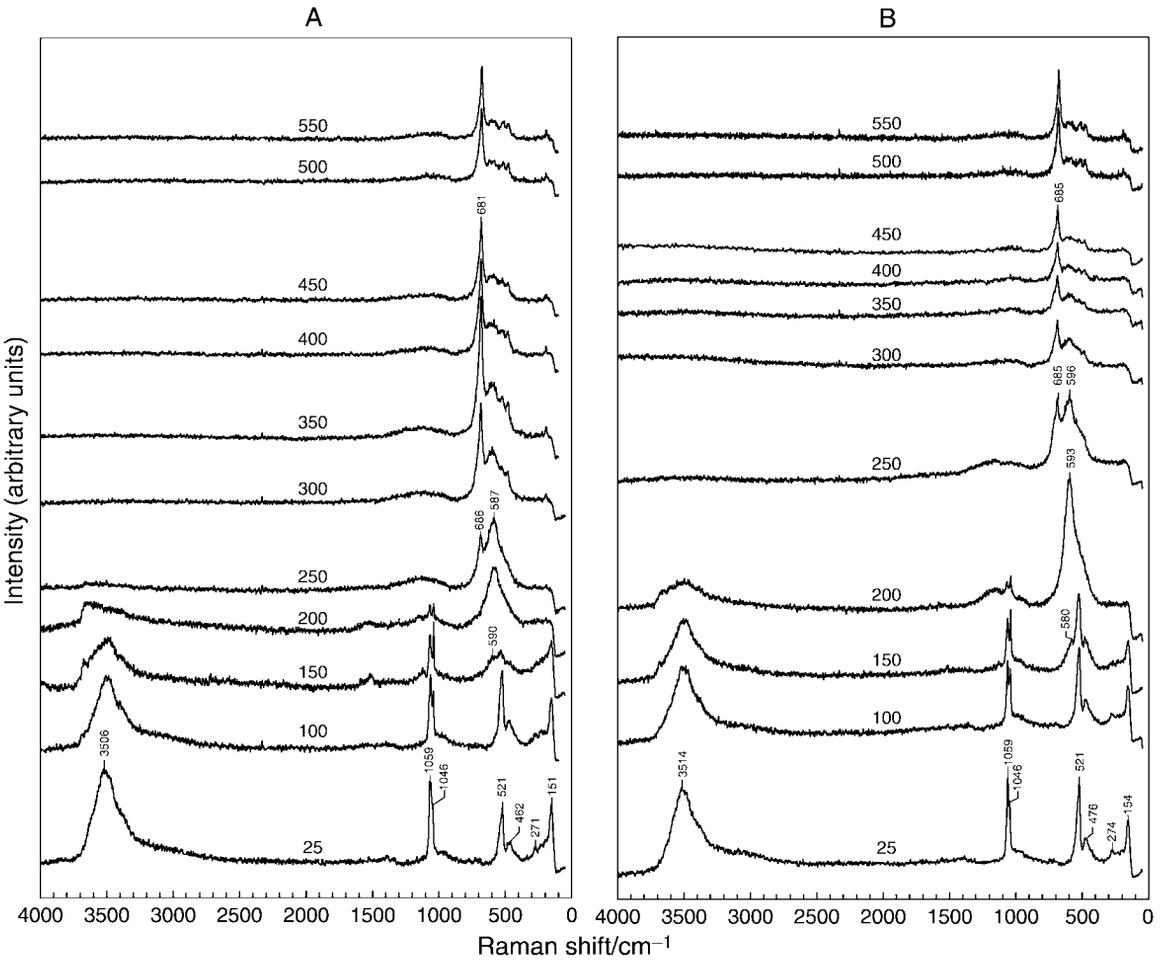

Fig. 6 *In situ* Visible Raman spectra for the thermal decomposition of Co–Al-HTlc (Co : Al = 3 : 1) in (A) air and (B) inert gas (N_2) at different temperatures (in °C), as indicated in the figure.

In situ visible Raman spectroscopy

Visible Raman spectra were recorded *in situ* during the decomposition of Co–Al-HTlc in both air and inert gas (Fig. 6). Analogously to the infrared analysis, the absorption band around 3500 cm^{-1} in the spectrum at room temperature is attributed to the H-bonded stretching vibrations of the hydroxyl groups of the brucite-like sheets, and stretching vibrations of water molecules. The shoulder around 3050 cm^{-1} in the infrared spectra, indicating CO_3^{2-}–H_2O bridging in the interlayer, is hardly visible in the Raman spectra at room temperature. The spectrum of Co–Al-HTlc contains a strong and sharp band at 1059 cm^{-1}, with a second band at slightly lower Raman shift (1046 cm^{-1}). The first band is assigned to in-plane OH bending vibrations, while the second band is attributed to the ν_1 mode (symmetric stretching) of the carbonate ions. The ν_4 mode of the carbonate, reported for Mg–Al-HTlc as a weak band at 694 cm^{-1},[25] was hardly visible in our spectra. Theoretically, the ν_2 and ν_3 bands are only infrared active and not Raman active. However, the Raman spectrum does show a very broad and low intensity band around 1400 cm^{-1}, corresponding to the infrared active ν_3 mode. This can be explained by the fact that the symmetry lowering of the carbonate interlayer site causes changes in polarizability, inducing Raman activity, although only with a very weak intensity.[23]

The low frequency region (<1000 cm^{-1}) of the spectrum at room temperature contains four bands. The bands at 521 and 492 cm^{-1} are both assigned to hydroxyl groups associated mainly with Al, both are probably also influenced by one Co in its coordination. The band at 492 cm^{-1} is only Raman active, while the band at 521 cm^{-1} has an equivalent in the infrared spectrum at 625 cm^{-1}. The bands at 154 and 274 cm^{-1} have not been previously assigned and may be due to framework vibrations, since they disappear at the same temperature as the layered double structure collapses.

The spectra obtained upon heating of the as-synthesized material have a straightforward interpretation. From room temperature to 150 °C, the spectra in air show the progressive removal of interlayer water and partial dehydroxylation (Fig. 6A). The bands at 1046 and 1059 cm^{-1} are also less intense, suggesting dehydroxylation and decarbonation, and the intensity ratio of the two peaks present is reversed with respect to the situation in the as-synthesized material. At 200 °C, the characteristic bands of the hydrotalcite phase are overlapped by a new sharp band at 593 cm^{-1}. The bands at 1046 and 1059 cm^{-1} further decrease in intensity and the shoulder at 3400 cm^{-1} disappears, indicating complete dehydration of the interlayer space. The bands at 154 and 276 cm^{-1}, related to framework vibrations of the layered structure are no longer visible at this temperature. The above-mentioned band at 593 cm^{-1} should be related to the emerging oxide phase and was assigned to a dispersed surface cobalt oxide phase.[37] This suggests an additional feature in the mechanism of formation of the oxide phase in Co–Al-HTlc. Apparently, the layered hydrotalcite loses hydroxyls upon heating, leading to a first (preliminary) oxide phase, where the cobalt is dispersed upon emerging cobalt aluminate or alumina (acting as a support). At 250 °C, the dehydroxylation of the sample is complete. At this temperature the intensity of the band at 590 cm^{-1} decreases and a new band appears at 685 cm^{-1}. This band is related to the formation of the oxide phase and thus to the collapse of the

Table 2 Summary of the transition temperatures (in °C) during the decomposition of Co–Al-HTlc (Co : Al = 3 : 1) in air and inert atmospheres obtained by different techniques

	Technique									
	HT-XRD		TGA-DSC		MS		FT-IR		Raman	
Transition	Air	Inert	Air	Inert	Air	Inert	Air	Inert	Air	Inert
Complete dehydration	150[a]	150	183	210	190	230	200	200	n.i.	n.i.
Collapse of the HTlc	200[b]	200–250[c]	n.i.	n.i.	n.i.	n.i.	250	350	150–200	150–200
Complete dehydroxylation	n.i.	n.i.	249[d]	270[d]	249	270	300	400	250	250
Complete decarbonation	n.i.	n.i.			375	*ca.* 600	500	>550	400	400

n.i.: not identified by this technique. [a]Observation of the metastable phase (coexistence of dehydrated layered structure and emerging cobalt oxide). [b]Leading ultimately to a mixture of Co_3O_4 and $CoAl_2O_4$. [c]Leading ultimately to a mixture of CoO and $CoAl_2O_4$. [d]Dehydroxylation and decarbonation cannot be identified separately.

layered structure. Complete decarbonation of the material is only identified around 400 °C.

The Raman spectra in inert gas show the same trend as the decomposition process as in air (compare Fig. 6A and 6B). The collapse of the layered structure occurs between 150–200 °C in air and 200–250 °C in inert gas. Furthermore, similar temperatures for complete dehydroxylation and decarbonation of the layered material in both atmospheres are obtained. These temperatures are slightly lower than those determined by other techniques. This suggests that, although the laser power was kept very low to avoid any extra heating of the material, a certain amount of damage to the sample cannot be completely prevented.

Combination of *in situ* techniques

As stated in the Introduction, most of the studies dealing with HTlcs and their partially decomposed products are performed *ex situ*. This reduces the value of the results, since ex-HTlcs have a strong tendency to rehydrate and further recover to the original structure by rehydroxylation of the brucite-like sheets (memory effect). Furthermore, the decomposition atmosphere markedly affects the decomposition mechanism of Co-hydrotalcite. The combination of *in situ* measurements presented in this paper provide excellent means to cope with these issues.

The *in situ* HT-XRD technique has only been applied for Mg-based HTlcs and is very suitable for the study of both the decomposition and reconstruction processes of the partially decomposed materials.[14,21,22] This technique gives substantial information on the different phases observed upon decomposition in air and inert gas, and thus provides insight into the differences in the decomposition mechanism. The different oxide phases formed in different atmospheres are obviously a consequence of the presence of oxidizable Co^{2+} in the brucite-like sheets of the layered material, as previously indicated.[18,44] This is expected based on the higher thermodynamic stability and free energy of formation of Co_3O_4 (compared to CoO) in air ($\Delta G_f^\circ = -795$ *vs.* -214 kJ mol^{-1}, respectively).[45]

A variety of interpretations are presented in the literature regarding the thermal analysis of hydrotalcites.[25,26,34,46] The discrepancies deal with the assignment of the two endothermal signals observed (I and II in Fig. 4). Kloprogge and Frost[25] assigned the first weight loss (RT–150 °C) to the removal of physically adsorbed and interlayer water. The endothermal transition I (150–212 °C) was assigned to complete decarbonation. The endothermal transition II (212–239 °C) was ascribed to the complete dehydroxylation of the sample. Finally, there is a residual weight loss (>239 °C), which was not assigned. The presented TGA-DTA profile is very similar to that shown in Fig. 3. Analysis of the gases evolved upon decomposition by mass spectrometry (Fig. 4) reveals that the thermal processes occurring are more complex than Kroprogge and Frost stated,[25] since the simultaneous occurrence of various transitions is involved. Dehydroxylation of the sample starts immediately after the removal of interlayer water and is coupled with the decarbonation stage, as was shown in the *m*/*z* 18 and 44 signals in Fig. 4. In this respect, Pesic *et al.*[19] also discussed interpretations by Miyata[34] for Mg–Al-HTlc. Thermal analysis requires the analysis of the evolved gases by MS in order to interpret the weight losses and endothermal transitions during decomposition properly.

The structural changes have also been nicely identified and substantiated by FT-IR and Raman spectroscopy. Classically, FT-IR has been applied in the identification of anions present in the interlayer space of hydrotalcite-like compounds.[1] Apart from this, information about the transitions of the single groups (water, hydroxyls, carbonates), changes in interactions between them (interlayer water–carbonates), and phase transitions can also be obtained. *In situ* visible Raman spectroscopy, applied for the first time to the study of the thermal decomposition of layered materials, has also been shown to be a powerful tool to further substantiate the results from *in situ* FT-IR spectroscopy and, in general, in combination with the other techniques presented here.

Table 2 summarizes the transition temperatures for the stages involved during thermal decomposition, as derived from the different analytical techniques applied in air and inert atmosphere. The results of the various techniques substantiate each other and, in general, are in good agreement. Complete removal of interlayer water is independent of the decomposition atmosphere. Collapse of the layered structure and complete dehydroxylation takes place at a relatively high temperature in inert gas, and decarbonation in particular occurs at much higher temperatures. Differences between the transition temperatures detected by different techniques in the same atmosphere are caused by different operation modes. Static techniques, *e.g.* HT-XRD, where the experiment is recorded after a certain equilibration time, lead to lower temperatures than dynamic techniques, with a continuous ramp of temperature during the measurement. The absolute values depend, however, on the applied heating rate (fixed at 10 °C min^{-1} in this study) and activation energy of the decomposition processes.

Structural model

Based on the analytical results obtained by the different techniques, the structural evolution of Co–Al-HTlc in air upon thermal evolution is illustrated in Scheme 1. The as-synthesized material is represented by three adjacent brucite-like sheets and the corresponding interlayer space (1). Physically adsorbed water is removed from the as-synthesized material below 100 °C. Simultaneously, release of some interlayer water is initiated, as is evident from HT-XRD and *in situ* FT-IR (2). Removal of interlayer water is complete in the range 150–200 °C, inducing a decrease in the basal plane (003) reflection. The finalization of this process in air leads to an intermediate

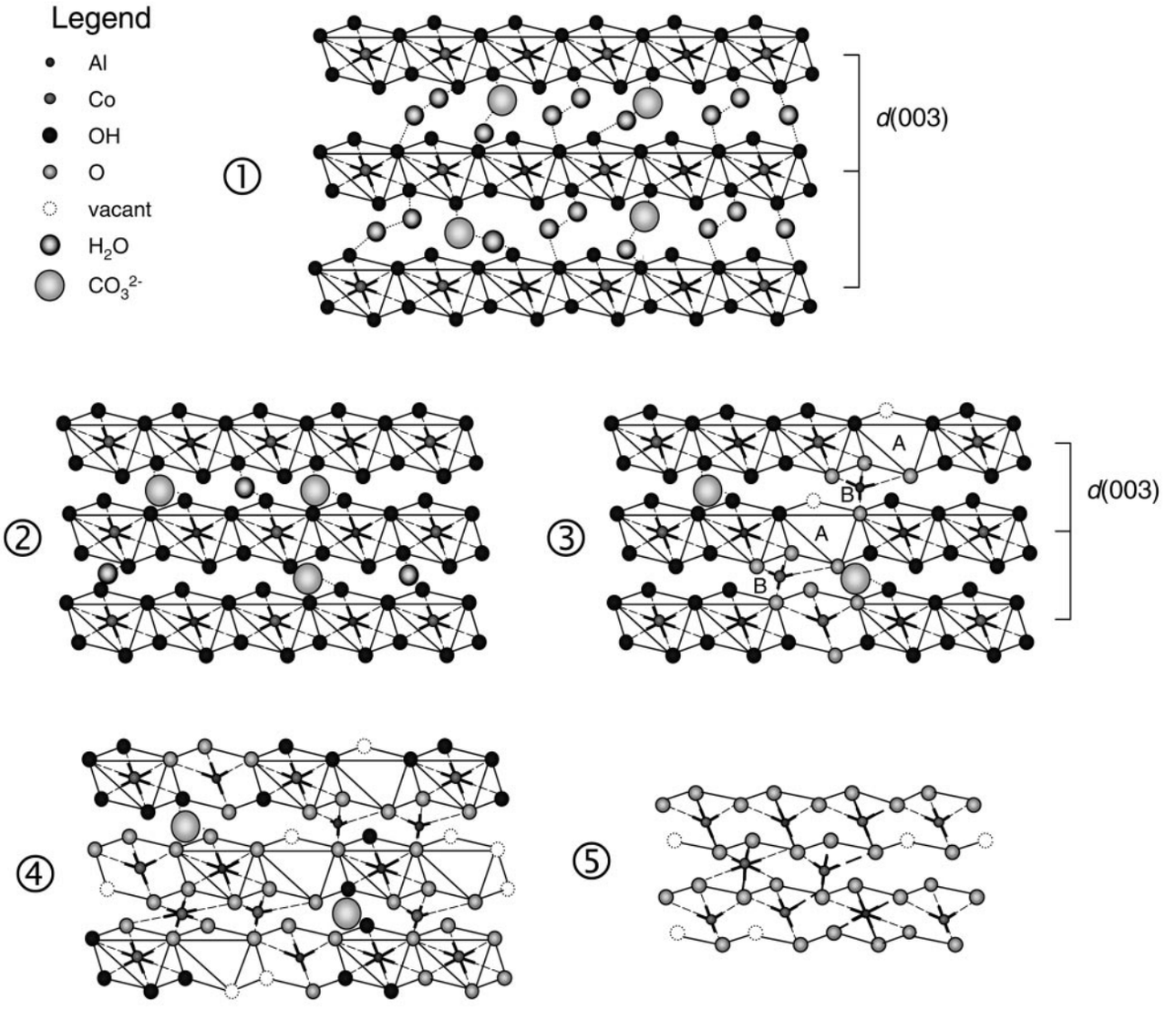

Scheme 1 Structural model for the decomposition of Co–Al-HTlc (Co : Al = 3 : 1) in air: (1) as-synthesized HTlc, (2) partially dehydrated HTlc, (3) metastable mixture of phases (dehydrated HTlc + emerging mixed oxide), (4) collapsed HTlc, and (5) oxide phase.

metastable mixture of phases, where the dehydrated hydrotalcite coexists with the solid solution of spinels $Co(Co,Al)_2O_4$ (3). The emerging mixed oxide phase observed in air indicates the partial oxidation of Co^{2+} to Co^{3+} and dehydroxylation of the brucite-like sheets to some extent at these low temperatures. At higher temperatures the hydrotalcite structure collapses completely and a solid solution of cobalt spinels is formed (4). Finally, dehydroxylation and decarbonation of the mixed oxide sample is complete (5).

The presence of oxidizable Co^{2+} cations in the octahedral layers of the as-synthesized material plays a decisive role in the decomposition mechanism. The oxidation of Co^{2+} to Co^{3+} in the presence of air may cause its diffusion to the interlayer space [from A to B in (3), Scheme 1]. As proposed by Belloto *et al.*,[14] removal of interlayer water promotes the diffusion of the trivalent Al^{3+} cation to the interlayer in Mg–Al-HTlc. This process leads to different cation coordination, changing to tetrahedral involving three oxygen atoms of the layer and one apical oxygen atom of the interlayer. According to these authors, the sites formerly occupied by the trivalent cation are left vacant, and the dimensions and geometry of the octahedral layer are maintained, which is in agreement with our results.

Our observations show the important role of the interlayer water in the decomposition mechanism, as anticipated by Belloto *et al.*[14] The dehydroxylation of the octahedral layers at temperatures where the metastable mixture of phases is observed (150 °C), as well as the oxidation of Co^{2+} to Co^{3+} and its diffusion to the interlayer space are limited as long as water is present in the interlayer space. This may induce dehydroxylation in the same layer. As we have shown elsewhere,[27] the metastable structure observed during decomposition in air recovers to the original layered phase after exposure to the ambient for 12 h. Above this temperature (> 150 °C) the interlayer is water-free, inducing a weaker interaction between the carbonates and the hydroxyls, as shown by infrared analysis.

Oxidation of Co^{2+} and diffusion of the Co^{3+} cation, as well as the intense dehydroxylation of the brucite-like sheet favours the formation of O–M–O bonds between layers (intralayer dehydroxylation), *via* the cation in position B, inducing the collapse of the layered structure and the formation of a stable mixed oxide phase $Co(Co,Al)_2O_4$ at low temperatures (*ca.* 200 °C). The stability of the solid solution of cobalt spinels prevents the retro-topotactic transformation to the hydrotalcite phase in wet feed gas or carbonated aqueous solutions after decomposition of Co–Al-HTlc at 200 °C.[27] Different authors have reported the oxidation process during drying or ageing of the coprecipitated Co-layered materials at relatively low temperature.[18,44] Xu and Zeng[47] have observed the oxidation process during the preparation of $Mg^{II}Co^{II}Co^{III}HT$ using a dynamic flow approach, where air was continuously supplied through bubbling to the liquid phase during the

precipitation step. The oxidation process $Co^{2+} \rightarrow Co^{3+}$ during thermal analysis of Co–Al-HTlc in air has also been identified; by the appearance of an exothermal signal at around 260 °C.[18,35] This signal was absent in an inert atmosphere.[18] In our case, this transition was not observed. A reasonable explanation was given by Uzunova *et al.*,[48] who suggested that the weak DTA signal caused by the oxidation process occurs simultaneously with thermolysis of the solid. As a result, the DTA signal due to carbonate and hydroxyl removal (endothermal) and that due to the oxidation process cancel each other out to some extent.

The decomposition mechanism is different in the absence of oxygen and should be similar to that of hydrotalcites with non-oxidizable cations, like Mg–Al or Ni–Al-HTlc. The decomposition model presented in Scheme 1 also applies in the case of an inert atmosphere, with the following modifications. In an inert gas, only Al^{3+} may diffuse to tetrahedral positions during decomposition, explaining the absence of the metastable phase during decomposition. The absence of Co^{2+} oxidation does not lead to the formation of a solid solution of cobalt spinels; here, phase separation is observed (CoO and $CoAl_2O_4$).

Conclusion

A combination of *in situ* techniques has been used to assess the thermal decomposition mechanism of Co–Al-HTlc in both air and inert atmospheres. HT-XRD, TGA-DTA, MS, *in situ* FT-IR spectroscopy and *in situ* Raman spectroscopy lead to a detailed description of the structural and physico-chemical transformations occurring upon heating the layered double hydroxide. Based on the information obtained by the different techniques, a structural model describing the decomposition mechanism has been proposed.

The presence of oxidizable Co^{2+} cations in the octahedral sheet leads to the formation of a highly stable and homogeneous solid solution of cobalt spinels upon decomposition in air, already identified at 150 °C. The diffusion of trivalent cations (Co^{3+}, Al^{3+}) to the interlayer space after removal of interlayer water favours the collapse of the layered structure through the formation of strong O–M–O bonds between layers. Co^{2+} oxidation was avoided by decomposition in inert atmospheres. Therefore, the collapse of the layered HT structure, as well as decarbonation and dehydroxylation processes, require higher temperatures.

Acknowledgements

This research was financially supported by the Council for Chemical Science of the Netherlands Organisation for Scientific Research (CW-NWO). G. M. gratefully acknowledges a fellowship granted by the Royal Netherlands Academy of Arts and Sciences. J. P. R. is indebted to M. M. Günter, T. Ressler, and O. Timpe for their assistance in the HT-XRD and MS experiments during his visit to the FHI, Inorganic Chemistry, Berlin. J. B. Taboada is acknowledged for performing the *in situ* FT-IR experiments.

References

1 F. Cavani, F. Trifirò and A. Vaccari, *Catal. Today*, 1991, **11**, 173.
2 J. Pérez-Ramírez, J. Overeijnder, F. Kapteijn and J. A. Moulijn, *Appl. Catal., B*, 1999, **23**, 59.
3 J. Pérez-Ramírez, F. Kapteijn and J. A. Moulijn, *Catal. Lett.*, 1999, **60**, 133.
4 A. Corma, V. Fornés, F. Rey, A. Cervilla, E. Llopis and A. Ribera, *J. Catal.*, 1995, **152**, 237.
5 J. J. Alcaraz, B. J. Arena, R. D. Gillespie and J. S. Holmgren, *Catal. Today*, 1998, **43**, 89.
6 S. Narayanan and K. Krishna, *Appl. Catal., A*, 1998, **174**, 221.
7 D. Tichit and F. Fajula, *Stud. Surf. Sci. Catal.*, 1999, **125**, 329.
8 K. K. Rao, M. Gravelle, J. Sanchez Valente and F. Figueras, *J. Catal.*, 1998, **173**, 115.
9 A. Corma, V. Fornés and F. Rey, *J. Catal.*, 1994, **148**, 205.
10 A. Alejandre, F. Medina, X. Rodriguez, P. Salagre and J. E. Suerias, *J. Catal.*, 1999, **188**, 311.
11 S. M. Auer, R. Wandeler, U. Göbel and A. Baiker, *J. Catal.*, 1997, **169**, 1.
12 P. S. Kumbhar, J. Sanchez Valente, J. M. M. Millet and F. Figueras, *J. Catal.*, 2000, **191**, 467.
13 M. Belloto, B. Rebours, O. Clause, J. Lynch, D. Bazin and E. Elkaïm, *J. Phys. Chem.*, 1996, **100**, 8527.
14 M. Belloto, B. Rebours, O. Clause, J. Lynch, D. Bazin and E. Elkaïm, *J. Phys. Chem.*, 1996, **100**, 8535.
15 R. Allmann, *Acta Crystallogr., Sect. B*, 1968, **24**, 972.
16 H. W. F. Taylor, *Miner. Mag.*, 1973, **39**, 377.
17 W. T. Reichle, S. Y. Chang and D. S. Everhardt, *J. Catal.*, 1986, **101**, 352.
18 M. A. Ulibarri, J. M. Fernández, F. Labajos and V. Rives, *Chem. Mater.*, 1991, **3**, 626.
19 L. Pesic, S. Salipurovic, V. Markovic, D. Vucelic, W. Kagunya and W. Jones, *J. Mater. Chem.*, 1992, **2**, 1069.
20 F. Rey, V. Fornés and J. M. Rojo, *J. Chem. Soc., Faraday Trans.*, 1992, **88**, 2233.
21 F. Millange, R. I. Walton and D. O'Hare, *J. Mater. Chem.*, 2000, **10**, 1713.
22 J. Rocha, M. del Arco, V. Rives and M. A. Ulibarri, *J. Mater. Chem.*, 1999, **9**, 2499.
23 J. T. Kloprogge and R. L. Frost, *J. Solid State Chem.*, 1999, **146**, 506.
24 B. Wu, S. Wang and Y. Zhuang, *Spectrosc. Lett.*, 1997, **30**, 1165.
25 J. T. Kloprogge and R. L. Frost, *Appl. Catal., A*, 1999, **184**, 61.
26 J. Pérez-Ramírez, G. Mul, F. Kapteijn and J. A. Moulijn, *Appl. Catal., A*, 2000, **204**, 267.
27 J. Pérez-Ramírez, G. Mul, F. Kapteijn and J. A. Moulijn, *Mater. Res. Bull.*, 2000, submitted.
28 A. S. Bookin and A. Drits, *Clays Clay Miner.*, 1993, **41**, 551.
29 M. del Arco, P. Malet, R. Trujillano and V. Rives, *Chem. Mater.*, 1999, **11**, 624.
30 D. Tichit, M. N. Bennani, F. Figueras and J. R. Ruiz, *Langmuir*, 1998, **14**, 2086.
31 J. T. Richardson and L. W. Vernon, *J. Phys. Chem.*, 1958, **62**, 1153.
32 S. Kannan and C. S. Swamy, *Catal. Today*, 1999, **53**, 725.
33 P. Grandvallet, Ph. Courty and E. Freund, *Proc. 8th ICC, Berlin*, Verlag Chemie, Weinheim, 1984, vol. II, 81.
34 S. Miyata, *Clays Clay Miner.*, 1980, **28**, 50.
35 T. Sato; H. Fujita, T. Endo, M. Shimada and A. Tsunashima, *React. Solids*, 1988, **5**, 219.
36 N. S. Puttswamy and P. V. Kamath, *J. Mater. Chem.*, 1997, **7**, 1941.
37 J. Pérez-Ramírez, G. Mul, F. Kapteijn and J. A. Moulijn, *Chem. Mater.*, 2000, submitted.
38 S. Miyata, *Clays Clay Miner.*, 1975, **23**, 369.
39 M. K. Titulaer, J. B. H. Jansen and J. W. Geus, *Clays Clay Miner.*, 1994, **42**, 249.
40 D. L. Bish and G. W. Brindley, *Am. Miner.*, 1977, **62**, 458.
41 M. J. Hernandez-Moreno, M. A. Ulibarri, J. L. Rendon and C. J. Serna, *Phys. Chem. Miner.*, 1985, **12**, 34.
42 F. M. Labajos, V. Rives and M. A. Ulibarri, *J. Mater. Sci.*, 1992, **27**, 1546.
43 J. Preudhomme and P. Tarte, *Spectrochim. Acta*, 1971, **27A**, 1817.
44 M. del Arco, R. Trujillano and V. Rives, *J. Mater. Chem.*, 1998, **8**, 761.
45 M. W. Chase, *Journal of Physical and Chemical Reference Data, NIST-ANAF Thermochemical Tables Part. 1. Al-Co*, Monograph 9, ACS, Washington, 1986, pp. 955, 957.
46 S. Kannan, S. Velu, V. Ramkumar and C. S. Swamy, *J. Mater. Sci.*, 1995, **30**, 1462.
47 Z. P. Xu and H. C. Zeng, *J. Mater. Chem.*, 1998, **8**, 2499.
48 E. Uzunova, D. Klissurski, I. Mitov and P. Stefanov, *Chem. Mater.*, 1993, **5**, 576.